

MODAL NOISE MITIGATION THROUGH FIBER AGITATION FOR FIBER-FED RADIAL VELOCITY SPECTROGRAPHS

RYAN PETERSBURG, TYLER MCCRACKEN, DOMINIC EGGERMAN, COLBY JURGENSON, DAVID SAWYER, DEBRA FISCHER
Department of Astronomy, Yale University, 52 Hillhouse Ave, New Haven, CT 06511, USA; ryan.petersburg@yale.edu

Draft version August 5, 2017

ABSTRACT

Optical fiber modal noise is a critically limiting factor for high precision spectroscopy signal-to-noise in the near-infrared and visible. Unabated, especially for highly coherent light sources, modal noise can induce radial velocity errors that hinder the discovery of low-mass (and potentially earth-like) planets. Previous research in this field has found sufficient modal noise mitigation through use of an integrating sphere, but this requires extremely bright light sources, a luxury not necessarily afforded calibration for the next-generation of high resolution optical spectrographs. Otherwise, mechanical agitation, which “mixes” the fiber’s modal patterns and allows the noise to be averaged over minutes-long exposures, provides some noise reduction but the methods have not been fully optimized by the community. Therefore, we have filled out the parameter space of modal noise agitation techniques in order to better understand agitation’s contribution to mitigating modal noise and to discover the optimal strategy for agitating fibers. We found that modal noise was best suppressed by the chaotic nature of coupled harmonic motion at high amplitude for fibers with large core diameters and low azimuthal symmetry, reducing modal noise induced radial velocity error to below 10 cm s^{-1} . This work has subsequently influenced the design of a fiber agitator to be installed with the Extreme Precision Spectrograph (EXPRES).



1. INTRODUCTION

Radial velocity (RV) exoplanet detection has continually been on the path of discovering less massive planets. The current goal of RV spectroscopy is 10 cm s^{-1} precision, thereby allowing the discovery of earth-like planets orbiting G and K stars in their respective habitable zone (Fischer et al. 2016). The next-generation of visible-band RV spectrographs—including but not limited to EXPRES (Jurgenson et al. 2016), ESPRESSO Mégevand et al. (2012), NEID (Schwab et al. 2016), and the Keck Planet Finder (Gibson et al. 2016)—require precision engineering and extreme stability to reach this goal.

Fiber coupling the spectrograph to the telescope has become an essential and standard method for planet hunting spectrographs enabling the spectrograph itself to be located in a controlled environment, isolating it from vibrational and thermal noise. Linking the telescope to the spectrograph via fiber also leverages the spatial scrambling properties inherent to fibers that, for the most part, decouple input variations from the output producing a stable illumination of the spectrograph optics (Hunter & Ramsey 1992). This effect has been amplified through the use of double scramblers (Halverson et al. 2015a; Spronck et al. 2015) and non-circular fiber geometries (Chazelas et al. 2010; Spronck et al. 2012; Plavchan et al. 2013).

Optical fibers also transmit light from calibration sources—such as wavelength calibrators and broadband flat-field sources—to the spectrograph. Laser frequency combs, especially the astrocomb (Probst et al. 2014) recently deployed at HARPS and soon at EXPRES, produce thousands of ultra-narrow, evenly spaced emission lines over a wide frequency range. When these highly coherent lines propagate through a multi-mode fiber, they create a source of noise that limits the signal-to-noise ra-

tio (S/N) of the instrument and potentially induces false signals into the data. This noise is caused by interference between the finite number of electromagnetic modes that can propagate along a multi-mode fiber, and has therefore been coined *modal noise*.

Some next-generation RV spectrographs—e.g. iLocater (Crepp et al. 2016) and M^{IN}ERVA-red (Blake et al. 2015)—have moved to a completely single-mode fiber architecture to help alleviate these complications. As apparent in their name, single-mode fibers only propagate a single electromagnetic mode and should be free from any modal noise. Due to the small core-size of single-mode fibers, however, coupling light from the telescope into these fibers is challenging and requires robust adaptive optics not currently available in the visible. Single-mode fibers also have a very limited bandwidth over which they propagate a single-mode meaning the fiber architectures for these spectrographs require multiple band-dependent paths. It is also possible that single-mode fibers are not free from modal noise since they propagate in two polarization modes that have been shown to affect spectrograph performance Halverson et al. (2015b). Thus, the study of modal noise reduction methods may still be necessary even regarding the existence of these novel single-mode fiber-fed instruments.

In this paper, we attempt to discern the optimal strategy for reducing modal noise using mechanical agitation on multi-mode fibers propagating coherent visible light. We begin by defining modal noise and exploring how previous experiments have mitigated it through static and dynamic methods (section 2). We then describe our own methods of fiber agitation (section 3) and discuss results from using these methods on fibers of varying cross-sectional shapes and coupling permutations (section 4). Finally, we relate these results to limits in RV precision (section 5) and discuss how these results should

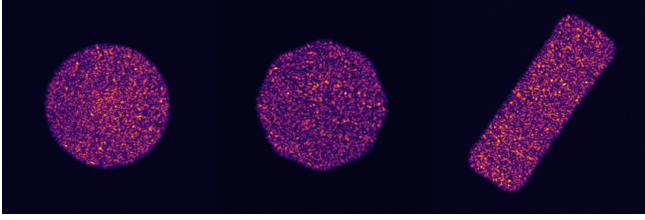


FIG. 1.— Examples of unmitigated modal noise for a 200 μm circular (left), 200 μm octagonal (middle), and 100 μm × 300 μm rectangular (right) optical fiber. All three fibers shown here have approximately the same cross-sectional area, meaning that they each are propagating about the same number of electromagnetic modes (see section 3). Brightness in this image is scaled by the $(\text{photon count})^{0.6}$ to better emphasize the fiber face. The contrast of the speckles is therefore *worse* than what is shown here.

be applied to next-generation RV spectrographs (section 6). The work in this paper was conducted to influence design decisions for EXPRES.

2. OPTICAL FIBER MODAL NOISE

Light propagates through an optical fiber in an integer number of electromagnetic modes. The exact calculation for this value is non-trivial since it depends on the instantaneous fiber geometry, injection parameters, and many other variables. The maximum number of modes for a step-index circular cross-section fiber (propagating a relatively large number of modes) is approximately given by

$$M_{circ} \approx \frac{4}{\pi^2} V^2 = \frac{4}{\pi^2} \left(\frac{2\pi r \text{NA}}{\lambda} \right)^2. \quad (1)$$

V is the normalized frequency of the fiber rewritten in terms of $\text{NA} = \sqrt{n_{core}^2 - n_{clad}^2}$, the numerical aperture of the fiber determined by the core (n_{core}) and cladding (n_{clad}) indices of refraction, the core radius r , and the wavelength λ of propagated light. This approximation is more difficult for a rectangular fiber, but Nikitin et al. (2011) shows empirically using electromagnetic and geometrical arguments that

$$\frac{M_{rect}}{M_{circ}} \approx 2 \frac{ab}{\pi r^2} \quad (2)$$

where a and b are the side lengths of the rectangular cross-section. Notice that ab and πr^2 give the areas for a rectangle and circle respectively. From this, we will assert more generally, with some re-arrangement of equation 1, that

$$M \approx C_s A \left(\frac{\text{NA}}{\lambda} \right)^2 \quad (3)$$

where A is the cross-sectional area of the fiber and C_s is a constant coefficient dependent on cross-sectional shape such that $C_{circ} \approx 16/\pi$, $C_{rect} \approx 32/\pi$, and is otherwise unknown for more complicated geometries.

When coherent light is propagated through a multi-mode fiber, a high contrast speckle pattern known as modal noise is produced at the output for both the near field (fiber face, figure 1) and far field (output pupil). Modal noise is an inherent property of all multi-mode fibers regardless of the cross-sectional core shape (Sablowski et al. 2015). It arises from light coupling from mode-to-mode as it propagates through fiber, causing

slight variances in the path length traveled and producing the observed interference pattern. For RV spectrographs this causes two problems: 1) it limits the maximum S/N and 2) systematic variations in the speckle pattern will mask themselves as minute shifts on the focal plane causing errant RV signatures.

2.1. Limit on S/N

Due to its high contrast, modal noise can severely decrease the S/N of an RV spectrograph (Epworth 1978; Baudrand & Walker 2001; Lemke et al. 2011). Light from the fiber is directly projected onto the spectrograph detector meaning any spatial variation in intensity of the injected light is evaluated as noise on the detector.

For a fiber without spatial filtering or a slit, the magnitude of this noise is proportional to \sqrt{M} (Goodman & Rawson 1981). Therefore, increasing the size of the fiber, increasing the numerical aperture of the fiber (or decreasing the injected focal ratio), and decreasing the wavelength of injected light should increase the S/N due to modal noise. It also appears that changing the fiber core shape could affect the S/N.

Experimental results of these conditions have been well documented. S/N due to modal noise has been shown to

- increase with larger fiber core cross-sectional area (Sablowski et al. 2015; Lemke et al. 2010)
- decrease with larger focal ratios (Sablowski et al. 2015; Baudrand & Walker 2001)
- decrease with longer wavelength of injected light (Baudrand & Walker 2001)
- slightly increase with more static bends in the fiber (changing the NA) (Imai & Asakura 1979)
- remain the same for fiber lengths greater than a few meters (Baudrand & Walker 2001)
- improve for non-circular fibers over circular fibers (Stürmer et al. 2016; Sablowski et al. 2015)

All of these results follow exactly from the above assumptions and implies that fibers with non-circular geometries have larger C_s .

2.2. Dynamic variations

In addition to being an issue of S/N, modal noise can induce false RV’s on the spectrograph since it is affected by dynamic optical properties (Mahadevan et al. 2014). If the speckle pattern drifts between exposures, especially with some period of motion, errant RV signatures could appear in the data.

As seen in equation 3, modal noise is heavily wavelength dependent. However, next-generation RV spectrographs are using stable wavelength calibrators rendering this problem effectively irrelevant. Otherwise, the speckle pattern seen at the end of a fiber changes over time most commonly because of (Epworth 1978):

1. temperature variation
2. fiber input illumination variation
3. fiber movement (bending, twisting, etc.)

These three conditions inevitably pose problems when imaging a spectrum since they are inherent to modern fiber-fed RV spectrographs (Baudrand & Walker 2001; Mahadevan et al. 2014). There is typically a temperature difference between the telescope and the spectrograph, fluctuations in atmospheric density and guiding change the fiber illumination, and the telescope (along with the connected fibers) slowly moves throughout the night.

2.3. Mitigation Techniques

Modal noise can be mitigated by continuously exacerbating one of the above three dynamic variations, thereby shifting the speckle pattern throughout an appropriately long camera exposure and averaging out the noise.  Controlled temperature variation (option 1) is non-ideal because a 1 meter fiber requires approximately 8°C fluctuations to visibly decorrelate the speckle pattern (Redding et al. 2013), and would be impractical to implement. Therefore, RV spectrographs have been left with either varying the illumination (option 2) or shaking the fiber (option 3).

As summarized in  Table 1, modal noise reduction techniques have been discussed by many experiments concerned with RV spectroscopy. These include methods that either vary the illumination or shake the fiber.

Mahadevan et al. (2014) and Halverson et al. (2014) explored the effectiveness of varying the illumination on the fiber face. Using an integrating sphere, diffuser, and rotating mirror, they showed gradual improvements in modal noise reduction due to the addition of further illumination variation. However, the integrating sphere, an integral part of these methods, has a throughput efficiency of approximately 10^{-6} and is not feasible to be introduced in the science light optical path. To allow flexible observing programs, particularly science observations bracketed by precision wavelength calibration sources, the modal noise mitigation technique needs to be more efficient.

Otherwise, the majority of these studies use various forms of agitation—including loudspeakers, paint mixers, and air streams—that shake the fiber over time. The variation in frequency and amplitude for these methods is unfortunately quite wide and conclusions are difficult to make. However, there have been slight trends in the results and the discussed assumptions so far are as follows:

- The frequency of agitation should be greater than $1/\tau$, where τ is the exposure time (Baudrand & Walker 2001).
- Noise is more effectively reduced by high amplitude motion (Lemke et al. 2011; McCoy et al. 2012).
- Higher frequencies (with an upper limit) show further noise reduction (Lemke et al. 2011).
- Adding a high frequency “tweeter” to a large amplitude “woofer” reduces noise further (Plavchan et al. 2013).
- Hand agitation is better than any form of mechanical agitation (Lemke et al. 2011; McCoy et al. 2012; Mahadevan et al. 2014; Roy et al. 2014).

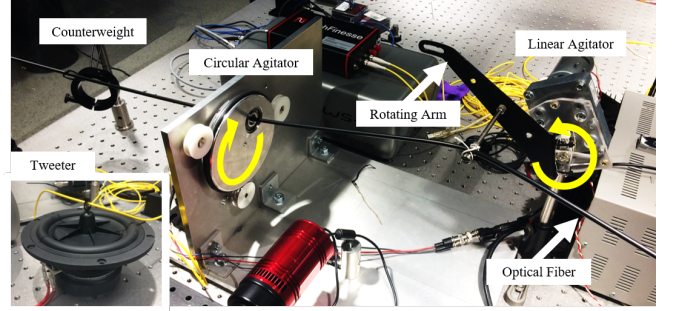


FIG. 2.— Laboratory images of the linear and circular agitator used in these modal noise tests attached to the $100\text{ }\mu\text{m} \times 300\text{ }\mu\text{m}$ rectangular fiber. The linear agitator rotates a variable-amplitude arm parallel to the fiber while the circular agitator rotates perpendicular to the fiber. A small counterweight keeps a minimal amount of tension in the fiber and prevents it from over-bending or bunching up. The inset in the bottom left contains a PASCO Scientific economy wave driver (“tweeter”) attached to an optical fiber. The tweeter is used to test high-frequency, low-amplitude agitation.

- Non-harmonic or chaotic motion is recommended (Grupp 2003) though an exact method has not yet been experimentally tested.

 Although this has been good for subjective intuition, the exact mechanisms behind the improvements in S/N and prevention of RV drift due to fiber agitation have not yet been explored.

In the following sections, we fill out the parameter space of fiber agitation methods further than previous studies. We are interested in seeing trends across different agitation amplitudes and frequencies, fiber shapes and sizes, and coupling permutations to make more precise conclusions about the nature of modal noise mitigation through fiber agitation.

3. EXPERIMENTAL SETUP

The number of modes a fiber supports is largely determined by its cross-sectional area (see equation 3).  In testing and characterizing agitation methods across multiple fiber geometries, we choose fibers with similar cross-sectional areas. Table 2 lists the fibers used in our experiment. Notice that the $200\text{ }\mu\text{m}$ circular, $200\text{ }\mu\text{m}$ octagonal, and $100\text{ }\mu\text{m} \times 300\text{ }\mu\text{m}$ rectangular fiber all have approximately the same cross-sectional area, meaning they can each support a similar number of modes.

Two different methods of large-amplitude mechanical agitation are used ( figure 2): the first produces a linear-type motion in which the fiber is moved up and down, the other is a circular type motion in which the fiber cross section is rotated perpendicular to the direction of propagation. The linear agitation has variable amplitude allowing for 80–320 mm agitation at 80 mm intervals and a variable frequency in the range of 0.03 to 1.0 Hz. For the circular agitator, the fiber is rotated in a circular path with a set amplitude of 80 mm and a variable frequency of 0.1 to 1.5 Hz. Routing a fiber through both agitators produces what we call “coupled agitation”. Frequencies are independently set by adjusting the appropriate DC-motor drive voltage and the amplitude of the linear agitator is set by the position of the lifting arm. A small counterweight is present to keep a minimal amount of tension in the fiber between the agitators and prevent it from folding on itself.

TABLE 1
PREVIOUS STUDY OF DYNAMIC MODAL NOISE MITIGATION METHODS

Reference	Method	Frequency	Amplitude
Daino et al. (1980)	Loudspeaker	110 Hz	“Sufficient”
Hill et al. (1980)	Turbulent Air Stream	—	—
Baudrand & Walker (2001)	—	30 Hz	1 mm
Lemke et al. (2011)	Loudspeaker	1.5 Hz	—
	Loudspeaker	80 Hz	—
	Paint mixer	60 Hz	—
McCoy et al. (2012)	Hand agitated	1-2 Hz	10-15 cm
	Mechanical agitator	“Low”	“High”
Plavchan et al. (2013)	“Tweeter”	100 Hz	1 mm
	“Woofer”	1 Hz	25 mm
	Int. Sph. + Diff.	—	—
Mahadevan et al. (2014)	McCoy agitator	“Low”	“High”
	Hand agitation	1-2 Hz	10 cm
Halverson et al. (2014)	Int. Sph. + Diff.	—	—
	Int. Sph. + OAP	—	—
Roy et al. (2014)	Rail agitator	“Low”	“High”
Sablowski et al. (2015)	Mechanical “Excenter”	2 Hz	20 cm

TABLE 2
TESTED OPTICAL FIBERS. ALL FIBERS HAVE NA = 0.22.

Shape	Size	Manufacturer
Circular	100 μm	Polymicro
Circular	200 μm	Polymicro
Octagonal	100 μm	CeramOptec
Octagonal	200 μm	CeramOptec
Rectangular	100 $\mu\text{m} \times 300 \mu\text{m}$	CeramOptec

TABLE 3
FIBER CHARACTERIZATION STATION IMAGING SPECIFICATIONS

Name	Camera	Pixel Size	Magnification
Input	Atik 450	3.45 μm	10
Near Field	Atik 450	3.45 μm	10
Far Field	Atik 383L+	5.4 μm	N/A

To test high-frequency, low-amplitude agitation, we use a PASCO Scientific “Economy Wave Driver” shown in the inset of figure 2. This device, attached to a sine wave function generator, produces approximately 5 mm amplitude for 10-30 Hz oscillations. It can be driven at higher frequencies, but the amplitude would not be large enough to produce significant fiber motion.

All image data is collected with the Fiber Characterization Station (FCS, figure 3), a multipurpose device that is able to simultaneously image the input face, output face (or near field), and output pupil (or far field) of the fiber under test. For these tests, we feed the FCS with either a 652 nm Toptica diode laser through a single-mode fiber or a broadband Thorlabs mounted LED centered at approximately 455 nm through a 100 μm circular fiber. Regardless of light source, the FCS focuses light into the fiber as a 10 μm circular spot. Specifications for the FCS cameras are listed in table 3. According to these specifications, our near field camera has a resolution of 0.3 μm , but after using statistical techniques on the fiber images, we have shown fiber-centering precision to about 0.01 μm .

Images exposure times are set according to the frequency of agitation such that each exposure lasts exactly one period of rotation. For example, if an agitator is set to rotate at 0.5 Hz, each image will be exposed for 2 s. We do this to confirm that only one full rotation is being recorded and allow for “number of rotations” to be another parameter for exploration.

Each data set is comprised of ten exposures for each of

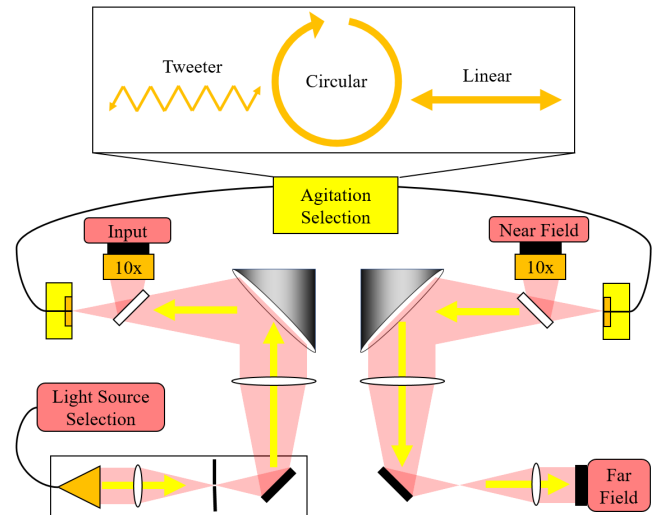


FIG. 3.— Schematic of the Fiber Characterization Station. Our choice of light source is fed into the station in the bottom left. This light is spatially filtered at focus, collimated, and finally injected into the test fiber as a 10 μm spot. The injection face of the test fiber is imaged at 10x magnification by the input camera to allow for precision alignment. Light propagates through the test fiber and our choice of agitator mixes the modes. A cartoon of the three types of agitation (see figure 2) is presented above the schematic. Light is then ejected from the test fiber and split between the 10x magnified near field camera and the far field camera.

the following cases:

1. the fiber being actively agitated
2. the fiber routed through the agitator but without agitation (“unagitated”)
3. the unagitated fiber illuminated with a broadband LED.

Multiple images are taken 1) to reduce statistical errors in our S/N calculations potentially caused by camera noise or small problems with our agitators and 2) to observe the effects of agitation at longer exposures time by co-adding multiple single-rotation images together. The LED source acts as a best-case scenario and the unagitated as a worst case.

We quantify modal noise using the S/N of light within

the fiber face of the near field image calculated as

$$S/N = \frac{\text{median}(I_{filt})}{\text{stdev}(I_0 - I_{filt})} \quad (4)$$

where I_0 , the original raw image, is heavily median filtered to produce I_{filt} . The typical S/N (where the “signal” is assumed to be a top-hat function across the fiber face) could not be used due to slight intensity-varying diffraction effects (see figure 6). Subtracting I_{filt} from I_0 therefore produces a noise pattern that reflects the modal noise and not these large-scale diffraction-caused variances. We use a circular 51-pixel median filter rather than a low-order polynomial or Gaussian fit because these latter functions could not sufficiently fit the raw fiber images. The size of the filter kernel was chosen such that speckles on unagitated images are sufficiently filtered without removing structure from the edges of the fibers. The numerator in equation 4 is calculated as the median (rather than the mean, for example) of I_{filt} to prevent dust on the fiber face or optics from skewing the S/N down.

We calculate the S/N for each individual image and average them together within each data set to yield a single-rotation S/N. We then co-add images 1-2, 1-3, ..., 1-10 and calculate the S/N for each case. The S/N for images 1-10 is presented as the ten-rotation S/N and each intermediate step as two-rotation S/N, three-rotation S/N, etc.

Far field images are taken for each data set and analyzed using the maximum intensity rather than the median intensity as the numerator in equation 4. The far field speckle pattern is of interest in precision RV spectroscopy as it is what illuminates the optics. However, mapping the far field speckle pattern to RV error would require numerical simulations with optical design software and is out of scope of this paper. That being said, all results listed in the following section may be extended to the far field though we omit the data for conciseness.

4. RESULTS

4.1. Method of Agitation and Fiber Geometry

We compare the two individual agitation methods and coupled agitation using all of the fibers listed in table 2. The linear agitator is set to an amplitude of 80 mm and the frequency of both agitators to 1.0 Hz. All images are taken with 1 s exposures.

Results for the single-rotation and ten-rotation cases are shown in figure 4. Across all fiber shapes and sizes and number of rotations, the linear agitator appears to be slightly better than the circular agitator. There is a similar increase in S/N when looking at coupled agitation in single-rotations. However, coupling the agitation over ten-rotations significantly increases the S/N for all fiber configurations.

To better understand why coupled agitation is more effective at reducing modal noise at longer exposures, we also analyze the effect of each agitation method over multiple rotations, as shown in figure 5 for the 100 μ m \times 300 μ m rectangular fiber. S/N shows continued improvement beyond a single rotation when coupling the agitation methods. The rate of this improvement is about the same (if not slightly better) than that when

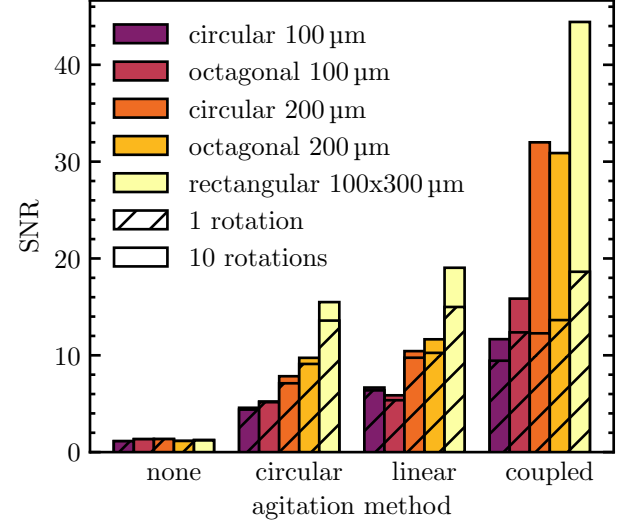


FIG. 4.— S/N comparison for varying fiber geometries and large-amplitude agitation methods. The S/N is presented for both single-rotation and ten-rotation images.

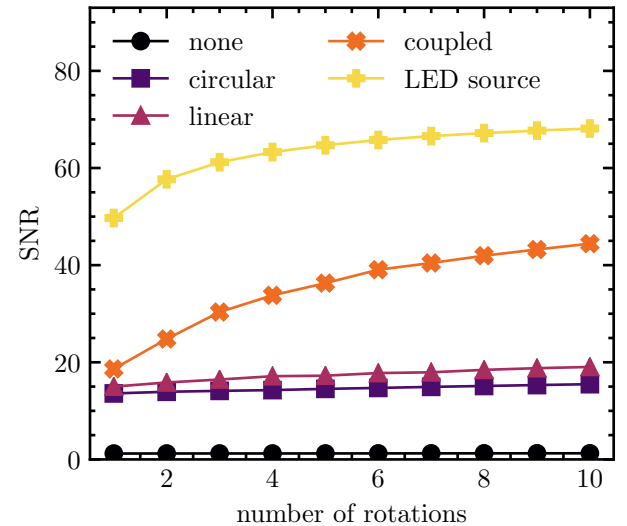


FIG. 5.— S/N dependence on number of rotations for the 100x300 μ m rectangular fiber using various agitation methods. We find similar relationships for the all of the remaining fiber shapes and sizes.

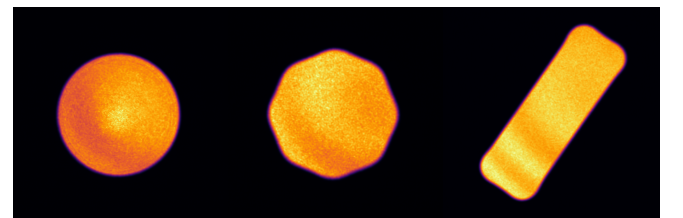


FIG. 6.— Ten-rotation, coupled agitation images using the same three fibers shown in figure 1. The diffraction pattern is clearly seen, but otherwise, the presence of speckles in these images is significantly diminished. Brightness is directly scaled with photon count in these images.

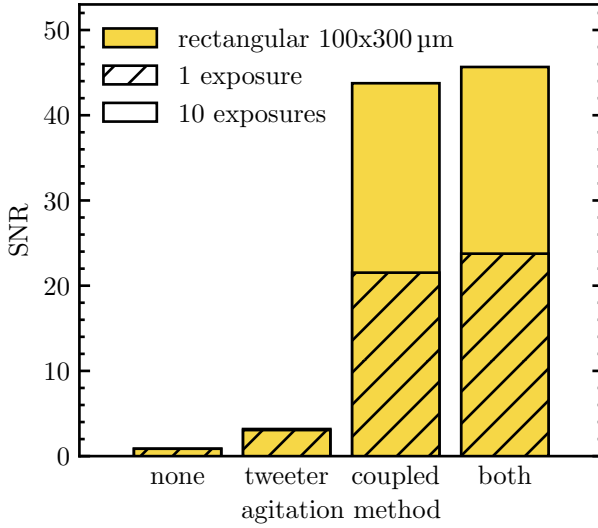


FIG. 7.— S/N comparison when adding a tweeter to the coupled agitation method for a rectangular fiber.

the fiber is lit by an LED, a broadband source. Circular and linear agitation, on the other hand, are effectively plateaued after the first rotation. We see identical effects for all of the remaining fiber shapes and sizes.

Ten-rotation images of the three larger fibers using the coupled agitation method are shown in figure 6. Compared to those shown in figure 1, the speckle patterns when using coupled agitation are nearly non-existent.

4.2. Adding a Tweeter

We also test the high-frequency, low-amplitude tweeter proposed by (Plavchan et al. 2013) in tandem with our coupled agitation to see if it supplies significant improvement to modal noise S/N. We only use the $100\text{ }\mu\text{m} \times 300\text{ }\mu\text{m}$ rectangular fiber for this test since it has so far yielded the largest response in . We set the linear agitator to 240 mm and 0.5 Hz and the circular agitator to approximately the same frequency. All exposure times are set to 2.0 s to match the rotation periods of the large-amplitude agitators.

The results are shown in figure 7. The tweeter slightly improves S/N regardless of exposure time when compared to the unagitated fiber and when added to coupled agitation. However, the magnitude of this improvement is minimal and is far outweighed by the improvement due to coupled agitation.

4.3. Amplitude and Frequency of Agitation

We use the $100\text{ }\mu\text{m} \times 300\text{ }\mu\text{m}$ rectangular fiber and the two agitators separately to test the effects of agitation amplitude and frequency of rotation on the S/N. We can only test amplitude on the linear agitator and take an image set for each position on the rotating arms. We test frequency on each of the linear and circular agitators at approximately equally spaced frequencies across their entire frequency range.

Results from these tests are shown in figure 8. There is a strong positive correlation between linear agitation amplitude using both the single-rotation and ten-rotation analyses. There also appears to be a slight increase in

TABLE 4
FIBER ASSEMBLIES TESTED FOR THE FIBER COUPLING EXPERIMENT

Test	1st Fiber	2nd Fiber
1	Circular 200 μm	Circular 200 μm
2	Circular 100 μm	Circular 200 μm
3	Octagonal 200 μm	Circular 200 μm

S/N for the linear agitator at higher frequencies after ten rotations, however there is no increase for the single-rotations or any of the frequencies when using the circular agitator.

4.4. Fiber Coupling

It is not uncommon for RV spectrographs to have multiple fiber links for carrying calibration and/or science light from the source (lamp or telescope respectively) to the spectrograph and ultimately detector. This results in having to couple light from one fiber to another and begs the question, is there a preferred fiber to agitate or must we agitate as many as possible? Agitating the first fiber in a multi-fiber system serves to vary the input illumination of subsequent fibers, similar to the methods proposed by Mahadevan et al. (2014) and Halverson et al. (2014). To study the effects of such an architecture, we agitate individual fibers in a multi-fiber assembly where each fiber could have different core sizes and shape. We test three distinct cases outlined in table 4 and compare them against agitating a single 200 μm circular fiber. For this test, fibers are agitated using the linear agitator at 80 mm and 1.0 Hz.

The results from these tests are shown in figure 9. For the most part, the S/N for each test hovers around 10, the same level at which the S/N would be for an uncoupled 200 μm fiber. However, the S/N when agitating only the 100 μm fiber is significantly less than 10. The single-rotation images when agitating the second fiber in the 200-200 μm test also seem to be abnormally low, but this appears to be repaired over longer exposures. Otherwise, the S/N when agitating both the coupled 200 μm octagonal and 200 μm circular fibers simultaneously is significantly improved.

4.5. Discussion

Our results can be summarized as follows: the highest S/N is attained when a fiber has been put through as many physical configurations as possible over the length of an exposure. This is best accomplished using a coupled agitation setup comprised of, in our case, linear and circular motion with the highest amplitude possible on each. Due to the coupled-harmonic motion of the two agitators, the resulting total agitation is effectively chaotic. One could conceive a single-element, random agitator as another possible implementation. Note that the motion needs to be continuous to avoid build-up of a static speckle pattern within the exposure.

This conclusion follows from some of the assumptions addressed in previous studies and introduced in section 2.3. Grupp (2003) actually recommended a chaotic high-amplitude agitator in his statistical study of modal noise. More recently, Lemke et al. (2011); McCoy et al. (2012); Mahadevan et al. (2014); Roy et al. (2014) found that hand-agitation is consistently better than any form of mechanical agitation. Human motions are inherently less deterministic than most mechanical devices thus re-

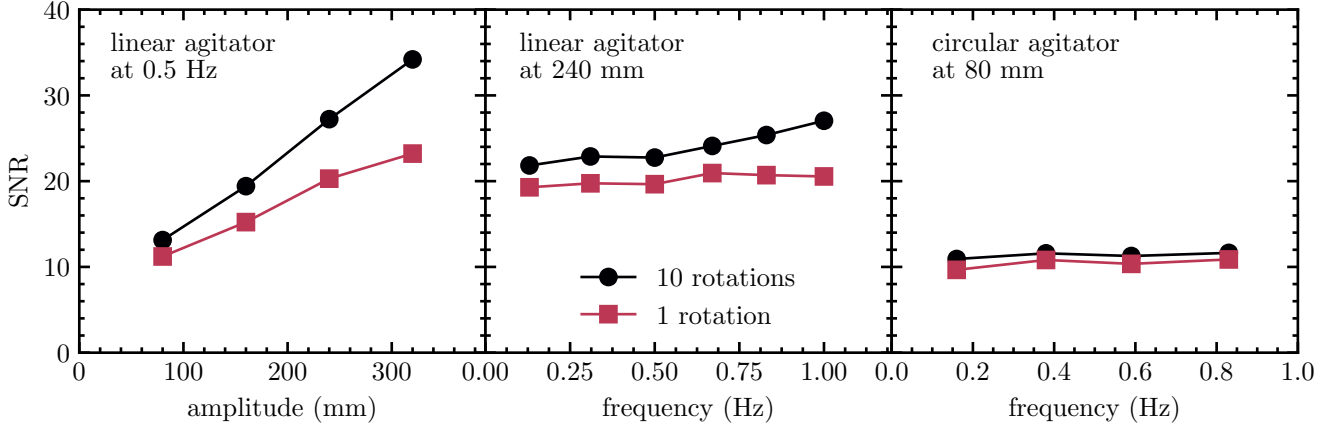


FIG. 8.— S/N comparison for varying amplitudes using the linear agitator (left) and varying frequencies using each of the linear (center) and circular (right) agitators.

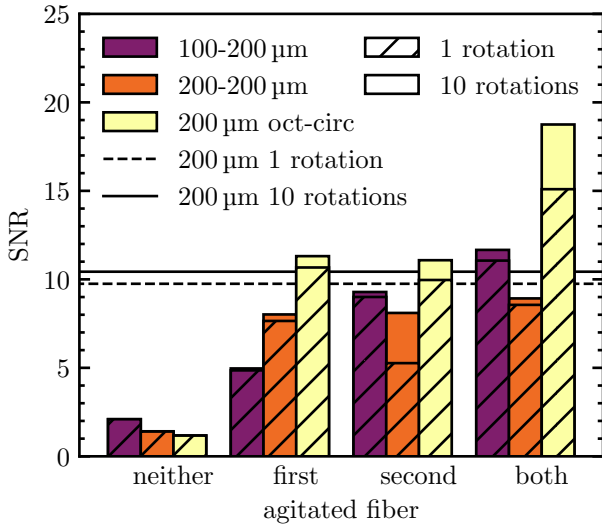


FIG. 9.— S/N for various arrangements of coupled fibers with varying core diameter and cross-sectional shape. All fibers can be assumed circular unless otherwise stated. The S/N for a single 200 µm circular fiber is also presented for both the single-rotation (dashed) and ten-rotation (solid) images.

sulting in a more chaotic motion. Our combined linear/circular agitator with slightly different oscillation frequency mimics this behavior since it chaotically reaches many fiber configurations.

Our results also strongly indicate that larger amplitude is much more crucial to mitigating modal noise than increased frequency, as clearly shown in figure 8. We continue to assert that any periodic rotation used as fiber agitation should complete its cycle within a single detector exposure as originally stated by Baudrand & Walker (2001). However, for single-element agitation, increasing the frequency does not show much of a discernible effect. We do note that the linear agitator does show a slight positive trend with frequency, but we believe this is caused by small random motions in the fiber further from the agitator that are indirectly intensified by the rapid motions of agitation.

Our tweeter tests also help show the importance of amplitude. Even though the high-frequency device is able to

place the fiber into many positions over a single exposure, the difference in these configurations is relatively small. Therefore, the speckle pattern is only “fuzzed” rather than averaged throughout the entire fiber face. Adding a tweeter to a large-amplitude agitator does show some small improvements (since extra “fuzzing” would naturally increase S/N), but these improvements are significantly overshadowed by simply having large amplitude motion.

We are also able to confirm previous results that show better mitigation of modal noise for fibers with larger cross-sectional areas and less azimuthal symmetry. As seen in figure 4, across all agitation methods, the 200 µm fibers fared better than the 100 µm fibers and the rectangular fiber was consistently far better than the others. Also, our derived expression for the number of modes (equation 3) accurately describes the ratio between each measured S/N shown in figure 4. For example, equation 3 predicts that doubling the diameter of a fiber should double the S/N, which is precisely reflected in figure 4. Also, we find that the rectangular fiber has approximately $\sqrt{2}$ times the S/N of the circular and octagonal fibers across all agitation methods since since $C_{rect} \approx 2C_{circ}$. Although there is no exact trend, the octagonal fibers tended to have a higher S/N than the circular fibers leading us to believe C_{oct} is slightly larger than C_{circ} .

It follows that the location of agitation in a fiber architecture should be on the fiber that propagates the most modes. We verify this as shown in figure 9. When coupling two fibers together that propagate the same number of modes, in our case a 200 µm circular fiber with itself and with a 200 µm octagonal fiber, there is no discernible difference in S/N when agitating one over the other. S/N is significantly worsened, however, when a smaller 100 µm circular fiber is agitated instead. Agitating both fibers appears to combine the improvements to S/N caused by agitating each fiber individually, but only when the two fibers have different size or geometry. When the two fibers are identical, S/N is unaffected.

Moreover, we can infer that location of agitation along a single fiber does not affect S/N. Coupling two 200 µm fibers with a 1:1 ratio is effectively adding their lengths together and creating a single fiber. As shown by figure

9, the location of agitation is irrelevant for such a situation, especially for ten-rotation exposures. Therefore, the agitator could be placed anywhere along the length of the fiber (preferably far away from the spectrograph) and it will produce the same magnitude effect on modal noise. This conclusion relies on only one test, however, so it will require further study to absolutely confirm.

Coupled fiber test cases with light loss due to improperly matched etendue, such as coupling light from a 200 μm fiber into a 100 μm fiber, were not covered for this paper and will require further study. However, we suspect that best modal noise mitigation will consistently occur when agitating the fiber that propagates the most modes, since improvements to modal noise S/N occur across the entire near field and far field projections and should be unaffected by truncation.

5. RADIAL VELOCITY PRECISION

As discussed in section 2, optical fiber modal noise is an issue of centroid drift as well as diminished S/N. To observe how the centroid actually drifts over time, we test our agitation method on the 100 μm × 300 μm rectangular fiber over three hundred 1.0 s exposures.

The resultant RV precision (σ_{RV}) due to a shifting speckle pattern centroid at the end of a fiber is calculated as:

$$\sigma_{RV} \approx \frac{c}{R D} \sigma_d \quad (5)$$

where c is the speed of light in a vacuum, R is the resolution of the spectrograph, σ_d is the standard deviation of fiber near field centroid drift in the dispersion direction and D is the slit width (or short-end length of a rectangular fiber). Importantly, σ_{RV} is only the RV error *per resolution element or per line* from a wavelength calibration source. Averaging over N lines, we can divide σ_{RV} by \sqrt{N} to approximate total RV error. Notice that for a $R = 150,000$ spectrograph fed by a 33 μm slit attempting to reach 1 m s⁻¹ RV precision per line, the required stability of the centroid along the dispersion direction is 0.0165 μm.

We derive equation 5 from the low velocity approximation of the relativistic Doppler effect

$$\frac{\Delta\lambda}{\lambda} = \sqrt{\frac{1+v/c}{1-v/c}} - 1 \approx \frac{v}{c} \quad (6)$$

where $\Delta\lambda$ is the measured shift in wavelength at wavelength λ on the spectrograph for a star moving at velocity v relative to Earth. The resolution of a spectrograph is

$$R = \frac{\lambda}{\Delta\lambda_R} \quad (7)$$

where $\Delta\lambda_R$ is the width of the spectrograph resolution element in terms of wavelength bandwidth. Centroid shifts in the near field of the fiber face can thus be equated to a measured wavelength shift at the focal plane of the spectrograph:

$$\frac{\Delta d}{D} = \frac{\Delta\lambda}{\Delta\lambda_R}. \quad (8)$$

Combining equations 6, 7, and 8 we show that

$$\frac{v}{c} \approx \frac{\Delta\lambda}{\lambda} = \frac{1}{R} \frac{\Delta\lambda}{\Delta\lambda_R} = \frac{1}{R} \frac{\Delta d}{D}. \quad (9)$$

If we take the standard deviation of the data from each side of this equation ($v \rightarrow \sigma_{RV}$, $\Delta d \rightarrow \sigma_d$) and move c to the right side, we get equation 5.

The idealized agitation method we use to test RV precision includes the circular agitator oscillating at 1.1 Hz and the linear agitation set at 240 mm and 1.0 Hz. Keeping the two agitators at slightly different frequencies means that a large range of fiber configurations are reached after about 10 s. We compare this idealized method to a broadband light source (low modal noise) and a slowly agitated fiber (high modal noise). For the slow agitation test, we set only the linear agitator at 80 mm and 0.03 Hz meant to mimic the slight motions of the telescope throughout a night.

We calculate the centroid of each image relative the center of the fiber in order to remove drift of the fiber stages. We also average these centroids over sets of 10 and 30 images to approximate the centroid drift for longer exposure times. For each length of exposure, we calculate the standard deviation of the centroid drift and convert this to a RV error using equation 5. The dispersion direction for a rectangular fiber is along the short end, meaning that the diameter D is 100 μm. The resolution of EXPRES is 150,000 for a 33 μm × 132 μm rectangular fiber, so we use $R = 50,000$ in equation 5 since our test fiber is three times as wide as the EXPRES fiber in the dispersion direction.

The results, shown in figure 10, indicate that coupled agitation reduces errors induced by a slow continuous agitation by about 3–5 times and are so far minimized to about 1.11 m s⁻¹ when using 30 s exposures. This error is the RV error per line in the spectrograph, meaning that the total RV error could be reduced to below 10 cm s⁻¹ with at least 120 lines. EXPRES is using a laser frequency comb with approximately 14 GHz line spacing leading to 250–450 lines per order on the spectrograph. This would reduce the RV error per order caused by modal noise to below 8 cm s⁻¹.

6. SUMMARY AND APPLICATION

We have tested a wide swath of agitation parameter space with the goal of further understanding the mechanisms behind fiber agitation as a method for modal noise mitigation. Our conclusions, as update to the previous assumptions introduced in section 2.3, are as follows:

- chaotic agitation, such as coupled harmonic motion, is much more effective at mitigating modal noise than typical harmonic agitation
- large amplitudes are crucial for this chaotic agitation
- for simple harmonic agitation, frequency is effectively irrelevant
- for chaotic agitation, the “frequency” should place the fiber into as many configurations as possible over a single exposure
- adding a “tweeter” shows minimal improvement over large-amplitude motion alone
- in a multi-fiber system, the fiber with the most propagating modes (see equation 3) should be agitated

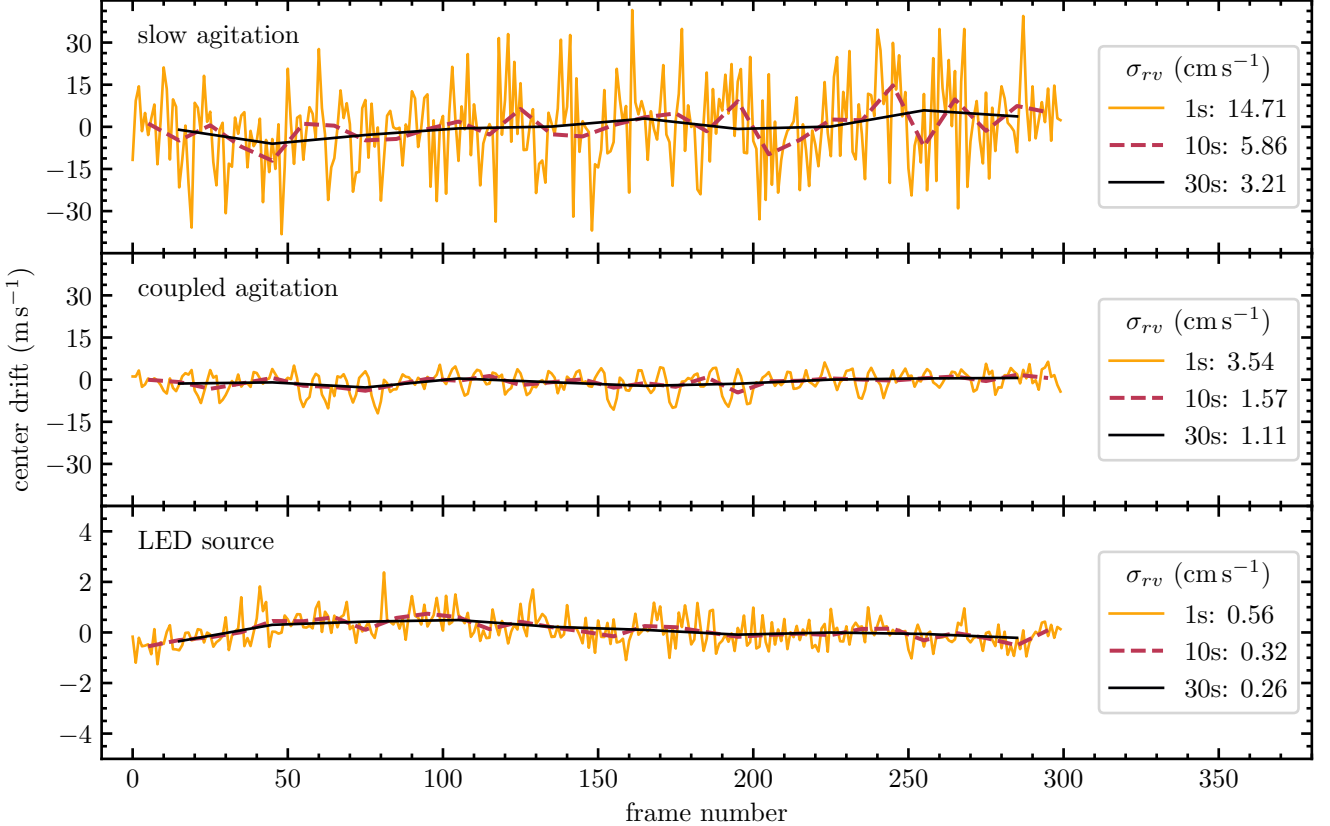


FIG. 10.— Centroid drift and resultant RV error for a slowly agitated fiber (top), coupled agitated fiber (middle), and LED illumination (bottom). Each line represents a different exposure time each with their own calculated RV error. Note that the scale for LED illumination is different from the other two to better show structure.



FIG. 11.— Comparison of the long-term agitation methods used in section 5—slow agitation (left), coupled agitation (middle), LED source (right)—as 10 s exposures. Brightness directly scales with photon count in these images.

As shown in figure 11, our chaotic coupled harmonic agitation method reduces modal noise to levels almost indiscernible from a fiber propagating broadband light after only 10 s. Since agitation hardly affects throughput efficiency, chaotic fiber agitation can therefore be used with relatively dim light sources, allowing for direct application to the next-generation of precision RV spectrographs.

It is important to note that there has not yet been a long-term study on how shaking an optical fiber may affect efficiency or the potentiality to completely break the fiber. Sablowski et al. (2015) demonstrate that focal ratio degradation is unaffected in the short-term and, so far, we have not heard any complaints from the RV spectroscopy community about fibers breaking due to agitation. However, any project that wishes to mechanically agitate fibers should take care to avoid over-bending or

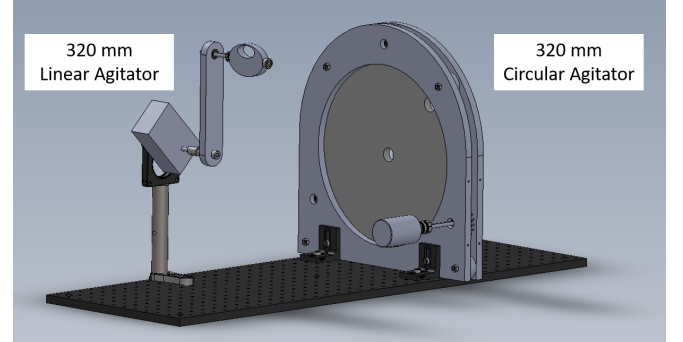


FIG. 12.— Rendering of the proposed fiber agitator for EXPRES. Both the linear and circular agitator have an independent DC motor operated by remote computer control. This agitator will sit on a shelf across the room from the spectrograph and will agitate all fibers that enter the spectrograph during both stellar and calibration exposures.

stretching their fibers and shake them with a minimal amount of aggression.

As part of the EXPRES fiber architecture, we will be employing the chaotic agitation technique detailed in this paper. We will be combining a 320 mm amplitude circular and linear agitator similar to those seen in figure 2, but with greater stability to support an entire reinforced wrap of cables. A rendering of this design is shown in figure 12. The two agitators will oscillate at slightly different frequencies at the maximum speed deemed safe for the fibers. This device will agitate all of the fibers

that immediately enter the spectrograph, which includes, most importantly, our rectangular fiber.

We recommend that other precision RV spectrographs consider the results found in this paper when designing their own fiber agitators. Since it only affects the fibers between light sources and the spectrograph, such improved agitation methods can even be added to previously commissioned spectrographs to improve S/N and reduce potential false positives. Modal noise is not a problem that should be treated lightly, and its mitigation will help usher in the next-generation of RV spectroscopy and aid in the search for Earth-sized worlds.

We would like to acknowledge NSF Major Research Instrumentation Award AST 1429365, as well as an NSF Advanced Technologies Instrumentation Award AST 1509436. The author would also like to acknowledge Gabor Furesz for assistance with the Fiber Characterization Station design as well as Saki Kamon, Kristoffer Acuña, and Dominic Eggeman for their data-taking contributions to this project. The Fiber Characterization Station was built with support from the Fund for Astrophysical Research, Inc. This material is based upon work supported by the National Science Foundation Graduate Research Fellowship under Grant No. 2017242370.

REFERENCES

- Baudrand, J., & Walker, G. A. H. 2001, Publications of the Astronomical Society of the Pacific, 113, 851 2, 3, 4, 7
- Blake, C., Johnson, J., Plavchan, P., et al. 2015, in American Astronomical Society Meeting Abstracts, Vol. 225, American Astronomical Society Meeting Abstracts, 257.32 1
- Chazelas, B., Pepe, F., Wildi, F., et al. 2010, in Proc. SPIE, ed. E. Atad-Ettedgui & D. Lemke, Vol. 7739, 47 1–9 1
- Crepp, J. R., Crass, J., King, D., et al. 2016, in Proc. SPIE, ed. C. J. Evans, L. Simard, & H. Takami, Vol. 9908, 19 1–13 1
- Daino, B., De Marchis, G., & Piazzolla, S. 1980, Optica Acta: International Journal of Optics, 27, 1151 4
- Epworth, R. 1978, in Fourth European Conference on Optical Communication (Genoa: Proceedings of the Fourth E.C.O.C., Genoa), 492–501 2
- Fischer, D., Anglada-Escude, G., Arriagada, P., et al. 2016, PASP, 45 1
- Gibson, S. R., Howard, A. W., Marcy, G. W., et al. 2016, in Proc. SPIE, ed. C. J. Evans, L. Simard, & H. Takami, Vol. 9908, 70 1–15 1
- Goodman, J. W., & Rawson, E. G. 1981, Optics Letters, 6, 324 2
- Grupp, F. 2003, Astronomy and Astrophysics, 412, 897 3, 6
- Halverson, S., Roy, A., Mahadevan, S., et al. 2015a, The Astrophysical Journal, 806, 1 1
- Halverson, S., Roy, A., Mahadevan, S., & Schwab, C. 2015b, ApJ Letters, arXiv:1511.02856 1
- Halverson, S., Mahadevan, S., Ramsey, L., et al. 2014, in Proc. SPIE, ed. S. K. Ramsay, I. S. McLean, & H. Takami, Vol. 9147, 1–6 3, 4, 6
- Hill, K. O., Tremblay, Y., & Kawasaki, B. S. 1980, Optics Letters, 5, 270 4
- Hunter, T., & Ramsey, L. 1992, Publications of the Astronomical Society of the Pacific, 104, 1244 1
- Imai, M., & Asakura, T. 1979, Optics Communications, 30, 299 2
- Jurgenson, C., Fischer, D., McCracken, T., et al. 2016, in Proc. SPIE, Vol. 9908 1
- Lemke, U., Corbett, J., Allington-Smith, J., & Murray, G. 2010, in Proc. SPIE, ed. E. Atad-Ettedgui & D. Lemke, Vol. 7739, 24 1–13 2
- Lemke, U., Corbett, J., Allington-Smith, J., & Murray, G. 2011, Monthly Notices of the Royal Astronomical Society, 417, 689 2, 3, 4, 6
- Mahadevan, S., Halverson, S., Ramsey, L., & Venditti, N. 2014, The Astrophysical Journal, 786, 1 2, 3, 4, 6
- McCoy, K. S., Ramsey, L., Mahadevan, S., Halverson, S., & Redman, S. L. 2012, in Proc. SPIE, ed. I. S. McLean & S. K. Ramsay, Vol. 8446, 8J 1–8 3, 4, 6
- Mégevand, D., Zerbi, F. M., Cabral, A., et al. 2012, in Proc. SPIE, ed. I. S. McLean & S. K. Ramsay, Vol. 8446, 1R 1–15 1
- Nikitin, P. V., Stancil, D. D., & Erosheva, E. A. 2011, in IEEE Antennas and Propagation Society, AP-S International Symposium (Digest), Vol. 2, 1662–1665 2
- Plavchan, P. P., Bottom, M., Gao, P., et al. 2013, in Proc. SPIE, ed. S. Shaklan, Vol. 8864, 0G 1–18 1, 3, 4, 6
- Probst, R. A., Lo Curto, G., Avila, G., et al. 2014, in Proc. SPIE, ed. S. K. Ramsay, I. S. McLean, & H. Takami, Vol. 9147, 1C 1–12 1
- Redding, B., Popoff, S. M., & Cao, H. 2013, Optics Express, 21, 6584 3
- Roy, A., Halverson, S., Mahadevan, S., & Ramsey, L. W. 2014, in Proc. SPIE, ed. S. K. Ramsay, I. S. McLean, & H. Takami, Vol. 9147, 1–7 3, 4, 6
- Sablowski, D. P., Plüsckie, D., Weber, M., Strassmeier, K. G., & Järvinen, A. 2015, Astron. Nachr., 1, 0 2, 4, 9
- Schwab, C., Rakich, A., Gong, Q., et al. 2016, in Proc. SPIE, ed. C. J. Evans, L. Simard, & H. Takami, Vol. 9908, 7H 1–6 1
- Spronck, J. F. P., Fischer, D. A., Kaplan, Z., et al. 2015, Publications of the Astronomical Society of the Pacific, 127, 1027 1
- Spronck, J. F. P., Fischer, D. a., & Kaplan, Z. a. 2012, in Recent Progress in Optical Fiber Research, ed. M. Yasin, S. W. Harun, & H. Arof (InTech), 353–370 1
- Stürmer, J., Schwab, C., Grimm, S., et al. 2016, in Proc. SPIE, ed. R. Navarro, Vol. 9912, 1T 1–7 2